Thin Solid Films 771 (2023) 139783

Contents lists available at ScienceDirect

Thin Solid Films

journal homepage: www.elsevier.com/locate/tsf

Enhancing the photocatalytic properties of doped TiO_2 nanowires grown by seed-assisted thermal oxidation

F. Giuffrida [a,b], L. Calcagno [a], A.A. Leonardi [a], M Cantarella [a], M. Zimbone [b,*], G. Impellizzeri [b]

[a] Department of Physics and Astronomy, University of Catania 95123 Catania, Italy
[b] CNR-IMM, Via S.Sofia 64 – 95123 Catania, Italy

ARTICLE INFO

Keywords:
Titanium dioxide
Nanowire
Ion implantation
Photoactivity
Iron doped
Platinum deposition

ABSTRACT

In the present paper, an investigation of the structural, optical, and photo-catalytical properties of TiO_2 nanowires (NWs) was conducted. The NWs were synthesized on a Si substrate by thermal oxidation of a thick (4 μm) Ti film covered by a thin (~ 5 nm) Au film. The annealing process at 750 °C produced a 1.7 μm thick NWs TiO_2 layer over a 3 μm thick TiO_2 film. Characterization techniques show that TiO_2 NWs are in rutile phase and have gold nanoparticles on top. Fe-doped TiO_2 NWs were synthesized to increase photoactivity in the visible range. The doping was performed using an unusual strategy, that is, implanting Fe^+ ions into the Ti layers before the growth of the TiO_2 NWs. The defectiveness introduced by the ion implantation is avoided and precise control of the doping is achieved. The photocatalytic properties were studied by following the degradation of methylene blue. In order to increase the photo-degradation rate under UV light of undoped NWs, two different strategies have been followed: 1) deposition of Pt nanoparticles on the front or on the rear side of the samples, and 2) thermal annealing in a reductive environment. A three-fold activity enhancement is obtained and discussed. Photocatalytic activity in the visible range was also measured for the Fe-doped samples, showing good activity, which was further improved by using the same strategies implemented under UV irradiation.

1. Introduction

Titanium dioxide (TiO_2) is an interesting material, especially for its photocatalytic properties [1,2]. This material finds several applications: in photocatalysis, photovoltaics, chemical sensing, and optical devices [3]. It can be used in super-hydrophilic and self-cleaning surfaces, and for water purification, as it can degrade the organic compounds absorbed on its surface when exposed to ultraviolet (UV) radiation [4]. The variety of applications arises from all the remarkable properties of TiO_2: good optical and electronic properties, long lifetime of excited electrons, long-term chemical stability, high corrosion resistance, and low cost.

The mechanism behind most of its applications is related to the delivery of photogenerated electrons and holes to the external environment and to the ability to decompose pollutants absorbed on the surface into non-toxic substances. Nevertheless, it is well known that the efficiency of TiO_2-based photocatalysis needs to be improved. In the literature, several strategies are used to improve the efficiency of this process [5–9]. For example, photo activity can be improved by

- increasing the exposed surface by the realization of nanoparticles, nanowires, or nanotubes [10–14]
- doping with metal and non-metal elements [15–18]
- reducing TiO_2 by H_2 [19–24]
- implementing fast laser processes for the formation of non-equilibrium nanoparticles [25,26]
- changing the oxygen partial pressure by self-doping with vacancies or with non-metal doping together [27–30]
- using noble metals such as Pt, Ag or Au as co-catalysts [31–34]
- employing the plasmonic properties of metallic nanoparticles [35]
- grafting Cu or Fe nanoclusters [36–41]

The small absorption of TiO_2 in the visible range is an issue that should be overcome: indeed, the wide band gap (about 3-3.2 eV) allows it to absorb only the UV light of the solar spectrum. The development of photocatalysts operating under visible light is particularly interesting, as it would allow the use of the full solar spectrum. Some authors have reported that doping the material with transition metals is an effective method to improve the response under visible light: the doping of bulk TiO_2 with Fe, Sb, or Cr by ion implantation has been demonstrated to

* Corresponding author.
E-mail address: massimo.zimbone@imm.cnr.it (M. Zimbone).

https://doi.org/10.1016/j.tsf.2023.139783
Received 5 September 2022; Received in revised form 2 March 2023; Accepted 2 March 2023
Available online 5 March 2023

produce a shift of the absorption band towards the visible light region [42–44]. For example, it has been demonstrated that implantation of TiO_2 thin film with Fe^+ ions generates local energy states under the conduction band, allowing the absorption under visible light, and inducing an improvement in photocatalytic efficiency [31]. Nano-structuration of the surface and the fabrication of nanowires, can further improve the pollutant degradation process thanks to the increase of surface/volume ratio that enhances the water/TiO_2 contact area and reduces the time for the charges to reach the surface.

In a previous paper, we investigated the growth of TiO_2 nanowires (NWs) by seed-assisted thermal oxidation [45]. The NWs were undoped, Pt nanoparticles were deposited on the rear side of the sample, and the photo-activity was investigated in the UV range. In this paper, we have deepened and developed the synthesis of doped Au-supported TiO_2 nanowires. We have investigated several strategies to improve the photocatalytic efficiency in both UV and visible range. A precise control of the uniformity and morphology is achieved. To induce a photocatalytic activity in the visible range, Fe^+ ions doping was carried out by ion implantation for the TiO_2 film before the NWs realization. The photocatalytic performances in both visible and UV ranges were further improved by depositing Pt nanoparticles on the front side of the sample and by an annealing in forming gas.

2. Materials and methods

Undoped NWs: A thick (~ 4 μm) film of titanium deposited by sputtering on a silicon substrate was used for the growth of TiO_2 nanowires. Samples were cut into pieces of about 1 cm x 1 cm then a thin gold layer (~ 5 nm) was deposited on the surface by using an RF (60 Hz) Emitech K550X as metalization sputtering system. The Au target has a 99.999% purity. The deposition was carried out in Ar flow at a current of 10 mA and a chamber pressure of 2 Pa (0.02 mbar). The 5 nm Au thickness was confirmed by Rutherford backscattering spectroscopy measurements using a 2.0 MeV He^+ beam. Thus the samples have been inserted into a covered quartz holder, and then TiO_2 NW synthesis was performed in 10 lpm of argon and 7.5 lpm of oxygen flux in a conventional furnace. The annealing was carried out in the temperature range of 600-750 °C, for 1.5 hr. Samples synthetized, as described, are called "TiO_2 NWs" or simply NWs. Some samples were further annealed in forming gas (95% of N_2 and 5 % of H_2). This annealing was performed at 500 °C with a gas flow of 7.5 lpm for 2 hrs. Samples annealed in forming gas are called "NWs + FG ".

Iron-doped NWs: Similarly to what is described in the previous paragraph, a thick (~ 4 μm) titanium film was deposited on a silicon substrate. Thus, the titanium films were implanted with Fe^+ ions at an energy of 150 keV (projected range 83 nm) and a fluence of 1.2×10^{16} ion/cm^2. Gold layer deposition and annealing in air were performed similarly to the unimplanted samples. Samples doped with iron are called "NWs + Fe ". Some doped samples were further annealed in forming gas and are called "NWs +Fe + FG ".

The synthesis of platinum nanoparticles (Pt NPs) was carried out by pulsed laser ablation in liquid with the same experimental apparatus and procedure described elsewhere [45]. Briefly, Pt nanoparticles solution was obtained by focusing (through a lens with focal length 20 cm) a laser beam (1064 nm, 10 ns) of a Q-switched Nd:YAG laser (Giant G790-30). The platinum metal plate (purity 99%) was purchased by Sigma Aldrich and is placed on the bottom of a teflon vessel filled with 2 ml of de-ionized water (MilliQ, Millipore, resistivity 18 MΩ·cm). The pulse energy was 337 mJ/pulse, and the fluence was estimated to be approximately 5 J/cm^2. Ablation was performed for 10 min. The nanoparticles, dispersed in water, remained stable for some years. The Pt nanoparticles were 20 nm in diameter, measured by dynamic light scattering. Pt nanoparticles deposition was carried out by drop-casting: 120 μl of the Pt NPs dispersion (corresponding to ~20 ug of Pt NPs) was deposited (drop by drop) at 90 °C on the front or back side of the samples. Before deposition on the back side, we polish the surface to remove the thin SiO_2 thermal oxide layer.

Scanning electron microscopy (SEM) analyses were performed by a Gemini field emission SUPRA 25 Carl Zeiss microscope operating at 3 -5 kV. The total reflectivity measurement was obtained using a Lambda 40 Perking-Elmer spectrophotometer. The band gap of the synthesized NWs was calculated using Kubelka-Munk and Tauc-Plot procedure [46]. Raman spectroscopy was carried out by using a micro-Raman Horiba Jobin Yvon HR550 system equipped with a 633 nm HeNe laser, with a 0.2 cm^{-1} resolution. The power of the laser was kept below 1 mW and an objective of 40x with 0.75 NA has been used. X-Ray Diffraction (XRD) analyses are performed with a Rigatu smartlab diffractometer at 0.5° angle of incidence, and θ-2θ from 20° to 60°.

The photocatalytic properties were studied by monitoring the degradation of the methylene blue (MB) dye in a de-ionized water solution at pH 7 under both UV and visible light. UV light was produced by a TL 8W BLB Philips lamp, with a peak at 368 nm (in the range of 350-400 nm) and an irradiance of 1.1 mW/cm^2 (measured at the sample surface). While the visible lamp emits in the range 400-500 nm with a peak at 454 nm (2.7 eV). Wavelengths lower than 400 nm were filtered out. The samples were placed vertically in closed cuvettes with the MB solution at a concentration of 10^{-5} M. The dye concentration was monitored "online" with a homemade apparatus by measuring the solution transmittance in the wavelength range of 630-700 nm. The equipment allows to measure 6 different cuvettes at the same time. Before the photocatalytic test, the samples were kept in the dark to allow the dye adsorbtion on the surface of the samples and cuvettes, then the samples were irradiated for a total time of 10 - 15 hrs. During the preconditioning period, in the dark, methylene blue concentration had no significant decrease, meaning a negligible absorption of MB onto the sample holder and on the sample surface. The MB concentration decay is fitted by a first-order decay function and the measured photocatalytic rate, K, was normalized by the sample area A (between 0.7-1.5 cm^2), so the value K/A is reported. Measurements are repeated 3 times and no changes in the photodegradation rate were found within the experimental errors.

3. Results

3.1. Undoped nanowires

The morphology and the structure of the TiO_2 NWs were studied by SEM analyses, optical spectroscopy, XRD, EDX and Raman spectroscopy. As reported in the experimental section, we had deposited 5 nm of Au film on 4 μm of Ti film and then we performed the annealing at different temperatures. Fig. 1 shows the SEM micrographs of the samples annealed in the temperature range of 600-750 °C for 1.5 h in flux (Ar at 10 lpm and O_2 at 7.5 lpm). The marker is the same for all the images. During the initial rise of the temperature in the annealing process, gold atoms on the substrate surface get mobility and thus the de-wetting of the (5 nm) continuous thin Au film occurs with the formation of nanoparticles.

In the annealed temperature range between 600 °C (a) and 650 °C (b), the Au nanoparticles come into sight and no clear nanowire formation is observed: between the two samples only small differences in morphology can be considered (see Fig. 1a and b, respectively). The formation of nanowires starts at 700 °C (c) and becomes evident at 750 °C (d). In particular, the sample annealed at 750 °C shows well-formed nanowires of about a micron-scale length: the fine structure of the nanowires is reported in Fig. 2a and b. Gold nanoparticles are visible on top of the NWs as already shown in [13,47]. Indeed, it is well known that Au catalyzes the growth of the TiO_2 NWs through Ti interstitial diffusion from the substrate [47]. At this temperature, NWs showed a rounded shape. Fig. 2 allowed us to evaluate the diameter distribution of the NWs (peaked at 90 nm). The surface density of the NWs was also estimated to be about 4.2×10^8 wires/cm^2. Fig. 2b in cross-view shows an "NWs film" thickness of about 1.7 μm. It is worth noting that, under

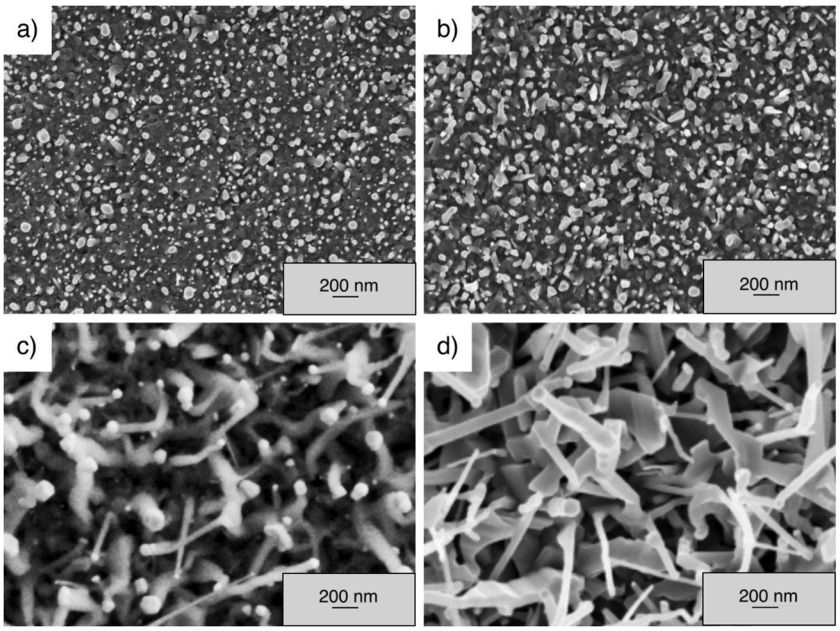

Fig. 1. SEM images in plan-view of the TiO_2 NWs grown at different temperatures 600° a) 650 °C b) 700 °C c) and 750 °C d) for a fixed annealing time of 1.5 hr. The marker is the same for all images.

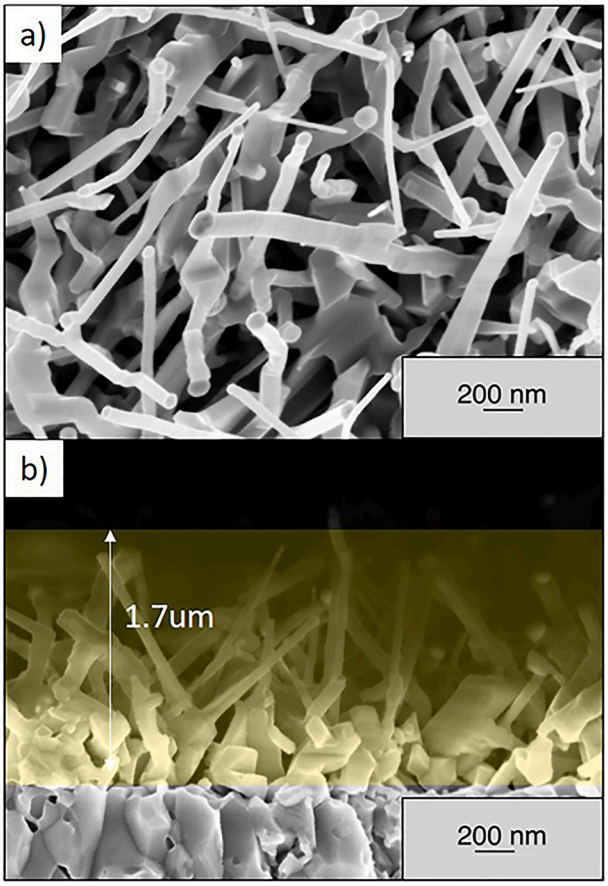

Fig. 2. SEM images in plan-view (a) and in cross-view (b) of the TiO_2 NWs grown at 750 °C for 1.5 hr.

the NWs, a TiO_2 compact layer (of 3 μm) and a ~ 2 μm of compact metallic Ti layer (under the TiO_2) are observable (not shown). The nanowires resulted tilted to the substrate, and the effective NWs length was estimated to be ~ 2 μm. Taking into account that NWs have a cylinder shape, it was possible to estimate a cylindrical surface area of about 4.8×10^{-9} cm^2 for every NW. By using the above-reported surface density of the nanowires (4.2×10^8 wires/cm^2), it is possible to roughly estimate the lateral surface of the overall nanowires (~ 2 cm^2).

Elemental EDX analysis was performed on the sample and the spectra confirm the presence of Au, Ti and O on the surface; no other contaminants are observed. Fig. 3 shows the optical characterization of the nanowires. In Fig. 3a, we report the apparent absorbance (1-Reflectance) spectra for the samples shown in Fig. 1. Only samples grown at 700 and 750 °C (in which nanowires are formed) have crystalline features: they are characterized by a high absorption at wavelengths lower than 400 nm. An analysis of these spectra, by using a Kubelka-Munk and Tauc-plot procedure, indicates a bandgap of about 3.1 and 3.2 eV for 700 and 750 °C samples, respectively, as expected for TiO_2 [48]. Information about the phase of the material were obtained by Raman and also XRD measurements. The Raman spectra reported in Fig. 3b showed the presence of two main peaks at 445 and 610 cm^{-1}, which are characteristic of the rutile phase of TiO_2, no peaks related to other phases are observed. Moreover, the Raman spectra evidenced the different quality of the two samples. Indeed, the Raman peaks are almost negligible in the 700 °C samples while they have high intensity and are well defined for 750 °C grown samples. The XRD spectra show the presence of the main peaks of the Rutile phase together with two peaks related to the gold nanoparticles (at about 38° and 44°). These Raman, XRD and UV-visible measurements confirm that Rutile is the only detected phase for nanowires growth with a seed-assisted methodology at 750 °C in O_2. The crystalline quality is improved by the higher annealing temperature, thus the samples annealed at 750 °C were chosen for further photoactivity investigations.

The photoactivity of the samples is evaluated by measuring the discolouration rate of a solution of MB in under UV and visible light irradiation. It has been fitted by a first-order decay function and normalized by the sample area A (about 1 cm^2). The discolouration rate K/A is reported in Fig. 4a for the different investigated samples. We refer to "Dye reference" for the dye solution without any samples, and "NWs" for the NW samples grown at 750 °C. In order to improve the photoactivity of the NWs, we deposited Pt nanoparticles on the surface of the samples. Nanoparticles are synthesized with a green and innovative technique

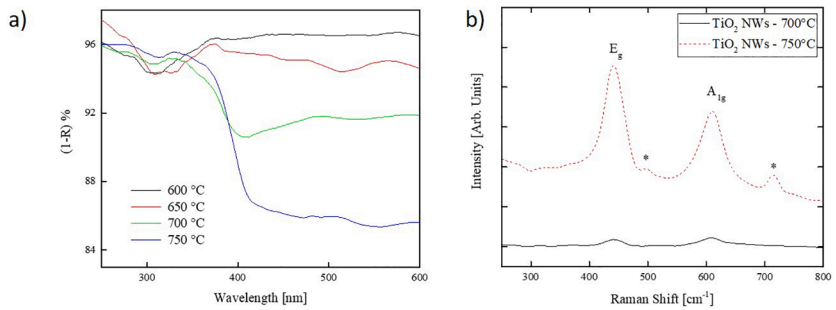

Fig. 3. Optical characterization of samples annealed at 600, 650,700 °C and 750 °C. a) Apparent absorption (1-R)% and b) Raman spectra are shown.

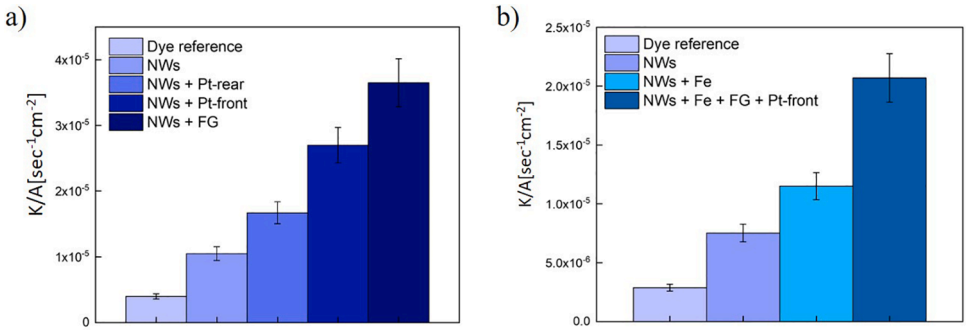

Fig. 4. a) UV-photocatalytic activity of different samples: Dye (without any catalyst), TiO_2 NWs, NWs with Pt on the rear, NWs with Pt on the front, and NW treated with forming gas. **b)** Visible photocatalytic activity of different samples: Dye (without any catalyst), TiO_2 NWs, NWs with Fe, NWs with Fe - FG- Pt on the front. The error bars represents the error in the reproducibility of the measurements.

such as the laser ablation in liquid (water) as reported in [45] and are characterized by a diameter of 20 nm and are fully stable in water solution after the synthesis. Nanoparticles were deposited by the drop-casting method, forming small clusters randomly distributed [21]. It is worth noting that the amount of the nanoparticles is under the detection limit of either the XRD and EDX techniques and moreover Raman spectra show no peculiar features related to Pt NPs nevertheless, they are visible in the SEM images.

In this work, we deposited nanoparticles on the front side or on the rear side of the sample. In Fig. 4a we report the photoactivity results of the degradation of MB dye with NWs enriched by Pt NPs. We called "Pt-rear" the NW samples grown at 750 °C and decorated with Pt NPs on the rear side while "Pt-front", the NW samples grown at 750 °C and decorated with Pt NPs on the front side of the samples. As shown in Fig. 4a, samples enriched with the Pt NPs are more active than the NWs samples and, the most photoactive samples are the ones with Pt NPs deposited on the front side. It has important implications as it will be discussed in the next section.

In Fig. 4a, the degradation rate of an NW sample annealed under forming gas ("NW+FG") flow at 500 °C for 2 hrs was also reported. The photoactivity showed a three-times improvement than the "NWs" sample. This sample is even more active than the Pt-front sample. The thermal annealing in a reductive environment (i.e., in our case forming gas), together with a low oxygen pressure, is well known to produce oxygen vacancies and/or Ti interstitials [28,29]. Moreover, the TiO_2 layer is in contact with the Ti layer and continuous injection of interstitials from the Ti layer to the TiO_2 is expected. The consequence should be a higher electron concentration in the conduction band bringing an improved conductivity [23,24]. These effects influence positively the NW photoactivity allowing electrons to be transferred to the scavenging sites with more efficiency.

3.2. *Fe-doped nanowires*

The samples used in the previous experiments show poor activity when illuminated with visible light as will be shown in this paragraph. This fact limits the possible application of the investigated NWs. In order to induce photoactivity in the visible range, we synthesized Fe-doped TiO_2 NWs. It was reported that Fe ion implantation in TiO_2 increases the conductivity of the film, introduces band gap states near the conduction band (able to absorb visible radiation), and thus increases the photoactivity in the visible range [44,50–54]. Nevertheless, in ion implantation methodology, a high flux of ions on the nanowires can cause the degradation of nano-structuration moreover even at low fluxes, this process introduces various kinds of defects such as vacancies and interstitials. Annealing (at high temperatures) is always necessary to restore the crystal quality, but it usually brings in the formation of complex defects (such as clusters and dislocation loops), with the consequent formation of deep levels. To avoid these difficulties, the strategy presente in the present paper is carried out. The ion implantation has been performed on the titanium film before the oxidation and thus before the formation of TiO_2 nanowires. In such a way, NWs grow from a substrate containing a defined amount of Fe, and so intrinsically doped. Fe^+ ions with an energy of 150 keV and a fluence of 1.2×10^{16} ion/cm^2 were implanted into Ti films. The chosen energy allows to contain the whole iron-implanted profile within the Ti layer: the Fe projected range is ~ 80 nm and the range straggle ~ 35 nm as obtained by STRIM [55] simulation. After the ion implantation, nanowires were grown as usual. Tacking into account that the solubility of Fe in TiO_2 is estimated to be 1% [56], Fe ions should diffuse uniformly in the oxide (i.e., into the 3 μm of TiO_2 film and 1.7 μm of TiO_2 NWs) and the final concentration can be estimated to be approximately 2.5×10^{19} ions/cm^3 (~ 0.1%). We checked the morphology and structure of the doped NWs. Two SEM images of the NWs formed with and without Fe doping are shown in the inset of Fig. 5. No actual difference is observed between these samples in SEM, Raman, EDX, and XRD measurements. Raman and

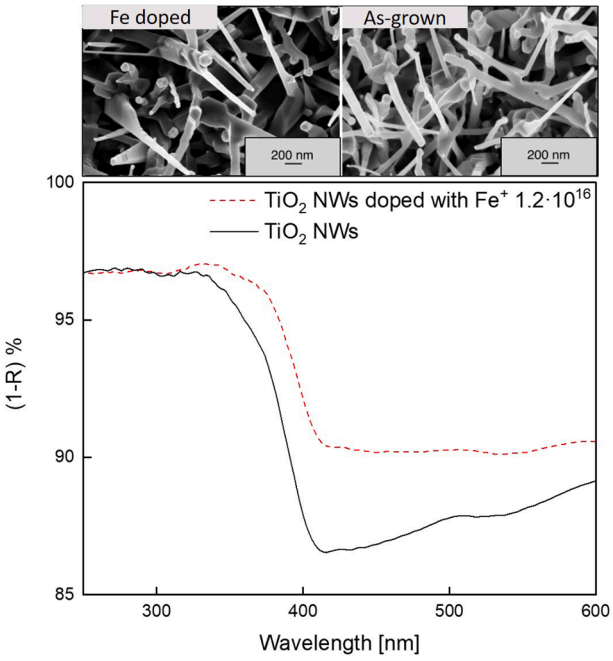

Fig. 5. UV-visible spectrum of the Fe-doped NWs compared with the undoped ones. Inset: SEM images of the NWs formed with and without the Fe doping.

XRD show that no change in the structure and vibration properties occurred in the doped samples compared to the undoped ones and no peaks related to the presence of iron are discernible in both cases. Only the UV-visible spectra and EDX spectra evidenced a small difference between the doped and undoped samples: In the EDX spectra, the presence of Fe peaks is detectable at about 6.5 KeV. The presence of iron also influences the UV-visible spectrum of NWs as compared with the undoped ones. In the UV-Visible spectra shown in Fig. 5, doped NWs show a higher base in the visible range and a different absorption offset at about 400 nm. The Fe-doped NW bandgap is evaluated to be about ~2.8 eV, which is slightly smaller than the undoped samples (~3.2 eV).

The Fe-doped NW photoactivity was then measured in the visible range. Fig. 6 shows the discolouration rate of the MB solution illuminated with visible radiation and the MB concentration as a function of time in the discolouration experiment, respectively. We measure a rate of 7.5×10^{-6} $s^{-1}cm^{-2}$ for the NW samples, while the Fe-doped NWs have 11.0×10^{-6} $s^{-1}cm^{-2}$, i.e.: "NWs Fe doped" showed an activity 1.5 times higher than undoped NWs.

In order to further improve the photocatalysis in the visible range, we modified the samples following the already discussed procedures: annealing in FG and the deposition of the Pt nanoparticles on the front side of the samples. An increment of about 2 times is observed in the discolouration rate: K/A increases from 11.0×10^{-6} to 21.1×10^{-6} $h^{-1}cm^{-2}$ by FG and Pt treatments. It is worth noting that a 3-fold increase is achieved compared to the bare TiO_2 NWs. This increase is due to either the Fe ions and the reduction due to the FG process. Although the Pt nanoparticles are present, their effect is considered to be less important than the effect of annealing in FG.

4. Discussion

Let's now discuss some features observed in the experiments. Briefly, the photocatalytic process is a complex phenomenon starting with the absorption of a photon by TiO_2 and the generation of an electron-hole couple. The photo-holes are transferred to liquid due to their high oxidation power while the photoelectrons accumulate into TiO_2 making the Fermi level of the TiO_2 more negative. An excess of electrons can thus recombine with holes non-radiatively or are transferred to solution through the dissolved molecular oxygen reduction (to superoxide, hydroxyl ion, hydrogen peroxide or water) [1–2]. The higher the transfer of electrons to solution the higher the activity in the degradation of contaminants such as MB. Therefore, to improve the photoactivity, we can act on several basic steps of this process: we focus our attention on two main steps, the absorption of the photons and the transfer of electrons to the solution.

Let's consider now the doping. We wanted to improve the small absorption of visible radiation in TiO_2 by doping. While TiO_2 has a bandgap of 3.2 eV, the iron-doped TiO_2 has a 0.4 eV lower value. This bandgap decrease can be related to the presence, in the Fe-doped TiO_2 NWs, of acceptor levels related to Fe^{+3} and donor Ti^{+3} states related to vacancies. Indeed, the introduction of iron (Fe^{+3}) in TiO_2 should be compensated by the formation of oxygen vacancies following the relation $Fe_2O_3 \xrightarrow{2TiO_2} 2Fe_{Ti}^{-1} + 3O_O^X + V_O^{+2}$ where we used the Kröger–Vink notation, in a similar way to the In incorporation in TiO_2 [57]. Radiation with an energy between 3.2 and 2.8 eV is allowed to be absorbed by the material. The photoactivity is, thus, improved as it is observed in Fig. 4b where "NWs with Fe" have a higher activity than the "NWs". Forming gas treatment has a similar effect to that obtained with iron doping indeed hydrogen induces the formation of Ti^{+3} states with consequently improved activity for TiO_2 [58]. This fact is evident in Fig. 4a where higher activity is observed after TiO_2 reduction in the FG atmosphere.

Another point to be considered is the effect of platinum. It is well known that Pt improves photoactivity, through the scavenging of electrons. Pt not only allows the formation of a Schottky junction at the metal/semiconductor interface but also, due to the high affinity of Pt with oxygen, catalyzes the oxygen reduction [49]. Interestingly, a large difference is found when the nanoparticles are deposited in the front or on the rear side of the sample as apparent in Fig. 4a. It shows that the rear side of the sample is not inert as is generally expected. On the contrary, the fact that deposition on the rear side improves the activity of the nanowires means that an electron current flows between the front and the rear side of the sample. In the case of the Pt nanoparticles deposited on the rear side, indeed a resistive voltage drop should be considered between the TiO_2 nanowires and the rear side of the sample where the nanoparticles are deposited. This resistance is clearly due to the sum of the resistances of the TiO_2 layer, the buried titanium layer, and the silicon substrate together with the contact resistance at the interfaces between these layers. The resistive voltage drops (related to the current between the front and the rear side) decrease (making it more positive) the Fermi level position of the nanoparticles on the backside of the sample. It also should reduce the over-potential on the rear side. Hence, the current that can be driven by the Pt nanoparticles decreases. This effect is absent for nanoparticles deposited on the front side, and thus they have a higher Fermi level position and a better scavenging effect, with improved activity. All the above-mentioned effects are exploited in the sample "NWs+Fe+FG+Pt front" which shows higher photoactivity in the visible range.

5. Conclusions

In conclusion, this paper presented the synthesis of TiO_2 nanowires and investigated some strategies to enhance the photocatalytic activity in both UV and visible ranges. NWs are obtained with an Au-catalyzed growth in an oxygen environment. They are in the rutile phase (with a bandgap of 3.2 eV), are 90 nm in diameter and 1 μm in length. The photocatalytic properties were studied by using the degradation rate of the methylene blue dye. To enhance photoactivity in the UV range, Pt nanoparticles were loaded and further annealing in forming gas was performed. The enhancement was more than three-fold and was related to the scavenging effect of the electrons by Pt nanoparticles and the increase of the conductance of the reduced TiO_2 phase. To activate the NWs in the visible range, TiO_2 NWs were doped with Fe^+ by ion implantation. The procedure is different from the commonly adopted one

in literature; indeed, we implanted the Fe^{+} ions into the Ti layer and then we realize the TiO_2 NWs. In such a way, we avoid the defectiveness introduced by the ion implantation technique. The photocatalytic activity of the doped samples was measured and they showed a good activity in the visible range. Similarly to the case of un-doped samples, the activity of doped samples is enhanced (doubled) after both annealing in forming gas and Pt nanoparticles loading.

CRediT authorship contribution statement

F. Giuffrida: Methodology, Formal analysis, Investigation, Data curation, Writing – review & editing. **L. Calcagno:** Conceptualization, Writing – original draft, Visualization, Supervision. **A.A. Leonardi:** Investigation. **M Cantarella:** Writing – review & editing. **M. Zimbone:** Conceptualization, Methodology, Formal analysis, Investigation, Data curation, Writing – original draft, Writing – review & editing. **G. Impellizzeri:** Validation.

Declaration of Competing Interest

The authors declare that they have no known competing financial interests or personal relationships that could have appeared to influence the work reported in this paper.

Data availability

Data will be made available on request.

Acknowledgements

The authors are grateful to P. Musumeci for the deposition of the Ti layer on Silicon and the support in the sample preparation. We acknowledge also G. Malandrino and F. La Via for the useful support in the XRD abd Raman measurements, and G. Pantè for his technical advice and support.

References

[1] A. Fujishima, X. Zhang, A. Tryk, TiO2 photocatalysis and related surface phenomena, Sur. Sci. Rep. 63 (2008) 515–582, https://doi.org/10.1016/j.surfrep.2008.10.001.

[2] H. Hashimoto, H. Irie, A. Fujishima, Photocatalysis: a historical overview and future prospects, Jap. J.l of Appl. Phys. 44 (2005) 8269–8285, https://doi.org/10.1143/JJAP.44.8269.

[3] T.S.Natarajan R.J.Tayade, H.C. Bajaj, Photocatalytic degradation of methylene blue dye using ultraviolet light emitting diodes, Ind. Eng. Chem. Res. 48 (2009) 10262–10267, https://doi.org/10.1021/ie9012437.

[4] H.Irie M.Miyauchi, M. Liu, X. Qiu, H. Yu, K. Sunada, K. Hashimoto, Visible-light-sensitive photocatalyst: nanocluster-grafted titanium dioxide for indoor environmental remediation, J. Phys. Chem. Lett. 7 (2016) 75–84, https://doi.org/10.1021/acs.jpclett.5b02041.

[5] K. Lee, H. Yoon, C. Ahn, J. Park, S. Jeon, Strategies to improve the photocatalytic activity of TiO2: 3D nanostructuring and heterostructuring with graphitic carbon nanomaterials, Nanoscale 11 (2019) 7025–7040, https://doi.org/10.1039/C9NR01260E, 2019.

[6] V. Etacheri, C. Di Valentin, J. Schneider, D. Bahnemann, S.C. Pillai, Visible-light activation of TiO2 photocatalysts: Advances in theory and experiments, J. Photochem. Photobiol. C Volume 25 (2015) 1–29, https://doi.org/10.1016/j.jphotochemrev.2015.08.003. December 2015.

[7] H.J. Yashwanth, S.R. Rondiya, N.Y. Dzade, R.L.Z. Hoye, R.J. Choudhary, D. M. Phase, S.D. Dhole, K. Hareesh, Improved photocatalytic activity of TiO2 nanoparticles through nitrogen and phosphorus co-doped carbon quantum dots: an experimental and theoretical study, Phys. Chem. Chem. Phys. 24 (2022) 15271–15279, https://doi.org/10.1039/D2CP01405J.

[8] M. Dorray, B.T. Goh, N.A. Sairi, P.M. Woi, W.J. Basirun, Improved visible-light photocatalytic activity of TiO2 co-doped with copper and iodine, Appl. Surf. Sci. 439 (2018) 999–1009, https://doi.org/10.1016/j.apsusc.2017.12.248, 1 May 2018.

[9] M. Alijani, B.K. Kaleji, S. Rezaee, Improved visible light photocatalytic activity of TiO2 nano powders with metal ions doping for glazed ceramic tiles, Opt. Quantum Electron. 49 (2017) 225, https://doi.org/10.1007/s11082-017-1064-x. Article number.

[10] R. Sanz, M.A. Buccheri, M. Zimbone, V. Scuderi, G. Amiard, G. Impellizzeri, L. Romano, V. Privitera Photoactive layered nanocomposites obtained by direct transferring of anodic TiO2 nanotubes to commodity thermoplastics, Appl. Sur. Sci. (2017) 399–462, https://doi.org/10.1016/j.apsusc.2016.12.037.

[11] G. Cacciato, M. Zimbone, F. Ruffino, M.G. Grimaldi, TiO2 nanostructures and nanocomposites for sustainable photocatalytic water purification, in: M. Larramendy, S. Soloneski (Eds.), Green Nanotechnology – Overview and Further Prospects, InTechOpen, 2016, pp. 87–116, https://doi.org/10.5772/62620.

[12] Y. Gao, X. Lin, Y. Zhao, S. Xu, C. Lai, Z. Guo, W. Wu, X. Ding, F. Jia, L. Zhou, Y. Liu, The cleaning effect of the photocatalysis of TiO2- B@anatase nanowires on biological activity on a titanium surface, Int.l J. Nanomed. 15 (2020) 9639–9655, https://doi.org/10.2147/IJN.S275373.

[13] E. Arcadipane, R. Sanz, M. Miritello, G. Impellizzeri, M.G. Grimaldi, V. Privitera, L. Romano, TiO2 nanowires on Ti thin film for water purification, Mater. Sci. Semicond. Process. 42 (2016) 24–27, https://doi.org/10.1016/j.mssp.2015.07.055.

[14] Y. Tang, H. Ren, J. Huang, Synthesis of porous TiO2 nanowires and their photocatalytic properties, Front. Optoelectron. 10 (4) (2017) 395–401, https://doi.org/10.1007/s12200-017-0735-3.

[15] M. Mrowetz, W. Balcerski, A.J. Colussi, M.R. Hoffmann, Oxidative power of nitrogen-doped TiO2 photocatalysts under visible illumination, J. Phys. Chem. 108 (2004) 17269–17273, https://doi.org/10.1021/jp0467090.

[16] Y. Zhang, C. Han, M.N. Nadagouda, D.D. Dionysiou, The fabrication of innovative single crystal N,F-codoped titanium dioxide nanowires with enhanced photocatalytic activity for degradation of atrazine, Appl. Catal. B: Environ. 168-169 (2015) 550–558, https://doi.org/10.1016/j.apcatb.2015.01.009.

[17] Y. Li, Y. Xiang, S. Peng, X. Wang, L. Zhou, Modification of Zr-doped titania nanotube arrays by urea pyrolysis for enhanced visible-light photoelectrochemical H2 generation, Electrochim. Acta 87 (2013) 794–800, https://doi.org/10.1016/j.electacta.2012.09.023.

[18] G. Impellizzeri, V. Scuderi, L. Romano, E. Napolitani, R. Sanz, R. Carles, V. Privitera, C ion-implanted TiO_2 thin film for photocatalytic applications, J. Appl. Phys. 117 (10) (2015), 105308, https://doi.org/10.1063/1.4915111.

[19] G. Wang, Y.Ling H.Wang, X.Yang Y.Tang, R.C. Fitzmorris, C. Wang, J.Z. Zhang, Y. Li, Hydrogen-treated TiO2 nanowires arrays for photochemical water splitting, Nano Lett. 11 (2011) 3026–3033, https://doi.org/10.1021/nl201766h.

[20] S.S. Pan, W. Lu, Y.H. Zhao, W. Tong, M. Li, L.M. Jin, J.Y. Choi, F. Qi, S.G. Chen, L. F. Fei, S.F. Yu, Self-doped rutile titania with high performance for direct and ultrafast assay of H2O2, Appl. Mater. Interfaces 5 (2013) 12784–12788, https://doi.org/10.1021/am4045162.

[21] M. Zimbone, G. Cacciato, R. Sanz, R. Carles, A. Gulino, V. Privitera, M.G. Grimaldi, Black TiOx photocatalyst obtained by laser irradiation in water, Catal. Commun. 84 (2016) 11–15, https://doi.org/10.1016/j.catcom.2016.05.024.

[22] M. Zimbone, G. Cacciato, M. Boutinguiza, A. Gulino, M. Cantarella, M. Privitera, V. Privitera, M.G. Grimaldi, Hydrogenated black-TiOx: a facile and scalable synthesis for environmental water purification, Catal. Today 321-322 (2019) 146–157, https://doi.org/10.1016/j.cattod.2018.03.040.

[23] X. Yan, L. Tian, X. Chen, Black Titanium Dioxide (TiO2). Nanomaterials. In Nanomaterials for Photocatalytic Chemistry, Y. Sun, World Scientific (2016), 1, 1-26. 10.1039/C4CS00330F.

[24] V. Scuderi, G. Impellizzeri, M. Zimbone, G. Nicotra, V. Privitera, Rapid synthesis of photoactive hydrogenated TiO2 nanoplumes, Appl. Catal. B: Environ. 183 (2016) 328–334, https://doi.org/10.1016/j.apcatb.2015.10.055.

[25] M. Zimbone, G. Cacciato, A.M. Buccheri, R. Sanz, N. Piluso, R. Reitano, F.La Via, M.G. Grimaldi, V. Privitera, Photocatalytic activity of amorphous hydrogenated TiO2 obtained by pulsed laser ablation in liquid, Mater. Sci. Semicond. Process. 42 (2016) 28–31, https://doi.org/10.1016/j.mssp.2015.09.012.

[26] M. Zimbone, G. Cacciato, M. Boutinguiza, V. Privitera, M.G. Grimaldi, Laser irradiation in water for the novel, scalable synthesis of black TiOx photocatalyst for environmental remediation, Beilstein J. Nanotechnol. 8 (2017) 196–202, https://doi.org/10.3762/bjnano.8.21.

[27] M.K. Nowotny, T. Bak, J. Nowotny, Electrical propweries and defect chemistry of TiO2 single crystal. I. electrical conductivity, J. Phys. Chem. B 110 (2006) 16270–16282, https://doi.org/10.1021/jp0606210.

[28] J. Nowotny, M.A. Alim, T. Bak, M.A. Idris, M. Ionescu, K. Prince, M.Z. Sahdan, K. Sopian, M.A.M. Teridi, W. Sigmund, Defect chemistry and defect engineering of TiO2-based semiconductors for solar energy conversion, Chem. Soc. Rev. 44 (2015) 8424–8442, https://doi.org/10.1039/C4CS00469H.

[29] M.K. Nowotny, L.R. Sheppard, T. Bak, J. Nowotny, Defect chemistry of titanium dioxide. application of defect engineering in processing TiO2-based photocatalysts, J. Phys. Chem. C 112 (2008) 5275–5300, https://doi.org/10.1021/jp077275m.

[30] A. Weibel, R. Bouchet, P. Knauth, Electrical properties and defect chemistry of anatase (TiO2), Solid State Ion 177 (2006) 229–236, https://doi.org/10.1016/j.ssi.2005.11.002.

[31] A. Tanaka, S. Sakeguchi, K. Hashimoto, H. Kominami, Preparation of Au/TiO2 with metal Co-catalysts exhibiting strong surface plasmon resonance effective for photoinduced hydrogen formation under irradiation of visible light, ACS Catal. 3 (2013) 79–85, https://doi.org/10.1021/cs3006499.

[32] G. Sanzone, M. Zimbone, G. Cacciato, F. Ruffino, R. Carles, V. Privitera, M. G. Grimaldi, Ag/TiO2 nanocomposite for visible light-driven photocatalysis, Superlatt. Microstruct. 123 (2018) 394–402, https://doi.org/10.1016/j.spmi.2018.09.028.

[33] G. Marzun, C. Streich, S. Jendrzej, S. Barcikowski, P. Wagener, Adsorption of colloidal platinum nanoparticles to supports: charge transfer and effects of

electrostatic and steric interactions, Langmuir 30 (2014) 11928–11936, https://doi.org/10.1021/la502588g.
[34] V. Scuderi, G. Impellizzeri, L. Romano, M.G. Grimaldi, V. Privitera, An enhanced photocatalytic response of nanometric TiO2 wrapping of Au nanoparticles for eco-friendly water applications, Nanoscale 6 (19) (2014) 11189–11195, https://doi.org/10.1039/C4NR02820A.
[35] A. Tanaka, K. Nakanishi, R. Hamada, K. Hashimoto, H. Kominami, Simultaneous and stoichiometric water oxidation and Cr(VI) reduction in aqueous suspensions of functionalized plasmonic photocatalysts Au/TiO2-Pt under irradiation of green light, ACS Catal. 135 (2013) 1886–1891, https://doi.org/10.1021/cs400433r.
[36] M. Liu, X. Qiu, M. Miyauchi, K. Hashimoto, Energy-level matching of Fe(III) ions grafted at surface and doped in bulk for efficient visible-light photocatalysts, J. Am. Chem. Soc. 135 (2013) 10064–10072, https://doi.org/10.1021/ja401541k.
[37] J.M. Kum, T.J. Park, H.J. Kim, S.O. Cho, Plasmon-enhanced photocatalytic hydrogen production over visible-light responsive Cu/TiO2, Nanotechnology 15 (2015), 125402, https://doi.org/10.1088/0957-4484/26/12/125402.
[38] M. Liu, X. Qiu, M. Miyauchi, K. Hashimoto, Cu(II) Oxide Amorphous nanoclusters grafted Ti3+ Self-doped TiO2: an efficient visible light photocatalyst, Chem. Mater. 23 (2011) 5282–5286, https://doi.org/10.1021/cm203025b.
[39] X. Qiu, M. Miyauchi, K. Sunada, M. Minoshima, M. Liu, Y. Lu, D. Li, Y. Shimodaira, Y. Hosogi, Y. Kuroda, K. Hashimoto, Hybrid Cux/TiO2 nanocomposites as risk-reduction materials in indoor environments, ACS Nano 6 (2012) 1609–1618, https://doi.org/10.1021/nn2045888.
[40] H. Irie, K. Kamiya, T. Shibanuma, S. Miura, D.A. Tryk, T. Yojoyama, K. Hashimoto, Visible light-sensitive Cu(II)-Grated TiO2 photocatalysts: activities and X-ray absorption fine structure analyses, J. Phys. Chem. C 113 (2009) 10761–10766, https://doi.org/10.1021/jp903063z.
[41] M. Miyauchi, H. Irie, M. Liu, X. Qiu, H. Yu, K. Sunada, K. Hashimoto, Visible-light-sensitive photocatalysts: nanocluster-grated titanium dioxide for indoor environmental remediation, J. Phys. Chem. Lett. 1 (2016) 75–84, https://doi.org/10.1021/acs.jpclett.5b02041.
[42] M. Zimbone, G. Cacciato, L. Spitaleri, R.G. Egdell, M.G. Grimaldi, A. Gulino, Sb-doped titanium oxide: a rationale for its photocatalytic activity for environmental remediation, ACS Omega 3 (2018) 11270–11277, https://doi.org/10.1021/acsomega.8b01452.
[43] K.A. Rahman, T. Bak, A. Atanacio, M. Ionescu, J. Nowotny toward sustainable energy: photocatalysis of Cr-doped TiO2: 2. Effect of defect disorder, Ionics 24 (2018) 327–341, https://doi.org/10.1007/s11581-017-2370-9.
[44] G. Impellizzeri, V. Scuderi, L. Romano, P.M. Sberna, E. Arcadipane, R. Sanz, M. Scuderi, G. Nicotra, M. Bayle, R. Carles, F. Simone, V. Privitera, Fe ion-implanted TiO2 thin film for efficient visible-light photo-catalysis, J. Appl. Phys. 116 (2014), 173507, https://doi.org/10.1063/1.4901208.
[45] M. Zimbone, M. Cantarella, G. Impellizzeri, S. Battiato, L. Calcagno, Synthesis and photochemical properties of monolithic TiO2 nanowires diode, Molecules 26 (2021) 3636, https://doi.org/10.3390/molecules26123636.
[46] P. Makuła, M. Pacia, W. Macyk, How to correctly determine the band gap energy of modified semiconductor photocatalysts based on UV–Vis spectra, J. Phys. Chem. Lett. 9 (23) (2018) 6814–6817, https://doi.org/10.1021/acs.jpclett.8b02892.
[47] E. Arcadipane, R. Sanz, G. Amiard, S. Boninelli, G. Impellizzeri, V. Privitera, J. Bonkerud, C. Bhoodoo, L. Vines, B.G. Svensson, L. Romano, Single-crystal TiO2 nanowires by seed assisted thermal oxidation of Ti foil: synthesis and photocatalytic properties, RSC Adv. 6 (2016) 55490–55498, https://doi.org/10.1039/C6RA09088E.
[48] J. Tauc, Optical properties of amorphous semiconductors, in: Amorphous and Liquid Semiconductors; J. Tauc, 4, Plenum Press, New York, 1974, p. 175.
[49] E. Kowalska, H. Remita, C. Colbeau-Justin, J. Hupka, J. Belloni, Modification of titanium dioxide with platinum ions and clusters: application in photocatalysis, J. Phys. Chem. C 112 (2008) 1124–1131, https://doi.org/10.1021/jp077466p.
[50] H. Wang, N. Zhang, G. Cheng, H. Guo, Z. Shen, L. Yang, Y. Zhao, A. Alsaedi, T. Hayat, X. Wang, Preparing a photocatalytic Fe doped TiO2/rGO for enhanced bisphenol A and its analogues degradation in water sample, Appl. Sur. Sci. 505 (2020), 144640, https://doi.org/10.1016/j.apsusc.2019.144640.
[51] J.H. Shen, H.Y. Chuang, Z.W. Jiang, X.Z. Liu, J.J. Horng, Novel quantification of formation trend and reaction efficiency of hydroxyl radicals for investigating photocatalytic mechanism of Fe-doped TiO2 during UV and visible light-induced degradation of acid orange 7, Chemosphere 251 (2020), 126380, https://doi.org/10.1016/j.chemosphere.2020.126380.
[52] G. Han, J.K. Kim, K.J. Kim, H. Lee, Y.M. Kim, Controlling surface oxygen vacancies in Fe-doped TiO2 anatase nanoparticles for superior photocatalytic activities, Appl. Sur. Sci. 507 (2020), 144916, https://doi.org/10.1016/j.apsusc.2019.144916.
[53] A. El Mragui, Y. Logvina, L. Pinto da Silva, O. Zegaoui, J.C.G. Esteves da Silva, Synthesis of Fe- and Co-Doped TiO2 with improved photocatalytic activity under visible irradiation toward carbamazepine degradation, Materials 12 (23) (2019) 3874, https://doi.org/10.3390/ma12233874.
[54] M. Crisan, D. Mardare, A. Iancelescu, N. Dragan, I. Nitoi, D. Crisan, L.Todan M. Voicescu, P. Oancea, C. Adomnitei, M. Dobromir, B.Vasile M.Gabrovska, Iron doped TiO2 films and their photoactivity in nitrobenzene removal from water, Appl. Sur. Sci. 455 (2018) 201–215, https://doi.org/10.1016/j.apsusc.2018.05.124.
[55] J.F. Ziegler, M.D. Ziegler, J.P. Biersack, SRIM - The stopping and range of ions in matter, Nuclear Instruments Methods Phys. Res. B 268 (2010) 818–1823, https://doi.org/10.1016/j.nimb.2010.02.091, 2013 version of the application is available at, http://www.srim.org/.
[56] J.P. Wittke, Solubility of iron in TiO2 (Rutile), J. Am. Ceram. Soc. 50 (1967) 586–588, https://doi.org/10.1111/j.1151-2916.1967.tb15004.x.
[57] J. Nowotny, M.A. Alim, A.J.Atanacio T.Bak, A. Malik, Electrical properties and defect chemistry of indium-doped TiO2: thermoelectric power, Ionics 201 (2015), https://doi.org/10.1007/s11581-014-1351-5, 5, 21, 2019-2029.
[58] Z. Wang, C. Yang, T. Lin, H. Yin, P. Chen, D. Wan, F. Xu, F. Huang, J. Lin, X. Xie, M. Jiang, H-doped black titania with very high solar absorption and excellent photocatalysis enhanced by localized surface plasmon resonance, Adv. Funct. Mater. 23 (2013) 5444–5450, https://doi.org/10.1002/adfm.201300486.